Available online at www.sciencedirect.com
SCIENCE DIRECT®
ELSEVIER
Journal of Sound and Vibration 275 (2004) 463–487
JOURNAL OF SOUND AND VIBRATION
www.elsevier.com/locate/jsvi

Optimal regularisation for acoustic source reconstruction by inverse methods

Y. Kim*,[1], P.A. Nelson

Institute of Sound and Vibration Research, University of Southampton, Southampton, SO17 1BJ, UK

Received 25 February 2003; accepted 30 June 2003

Abstract

An important inverse problem in the field of acoustics is that of reconstructing the strengths of a number of sources given a model of transmission paths from the sources to a number of sensors at which measurements are made. In dealing with this kind of the acoustical inverse problem, the strength of the discretized source distribution can be simply deduced from the measured pressure field and the inversion of corresponding matrix of frequency response functions. Hence, the accuracy of reconstruction of the source strength is crucially dependent on the conditioning of the matrix to be inverted. However, the problem of reconstructing acoustic source distributions from field measurement is very often ill-posed. In such cases, by using only the simple least-squares method, one cannot ensure a successful reconstruction of the acoustic source strength distribution. Therefore, Tikhonov regularisation is widely employed in order to produce reasonable solutions. However, determination of the amount of regularisation is not straightforward in practical applications without prior knowledge of either the strength of the acoustic sources or the contaminating measurement noise. Thus, two methods have been introduced, Generalised Cross Validation (GCV) and the *L*-curve method, which do not require prior information in order to determine the optimal regularisation parameter. In the present work, the abilities of the two methods are illustrated when these kinds of inverse sound radiation problems are dealt with using Tikhonov regularisation. Finally, through experimental demonstrations, some guidelines are proposed for determining the optimal degree of regularisation.

*Corresponding author. Tel.: +82-31-280-8146; fax: +82-31-280-9158.
E-mail address: ykim65@dreamwiz.com (Y. Kim).
[1] Present address: Samsung Advanced Institute of Technology (SAIT), Giheung-eup, Yongin-si, Gyeonggi-do 449-712, South Korea.

0022-460X/$ - see front matter © 2003 Elsevier Ltd. All rights reserved.
doi:10.1016/j.jsv.2003.06.031

1. Introduction

The reconstruction of acoustic source strength is important in order to provide understanding of source characteristics, such as source locations, source strengths and interactions between the sources. Such research has also been conducted with the purpose of the specification of the sound radiation process, appropriate noise control measures and the ranking of the contribution of multiple sources. The general objective is to establish these parameters in order to improve acoustic quality. Therefore, the study of acoustical inverse problems, a relatively new branch of the field of acoustics, is of considerable importance. In order to deal with this kind of acoustical inverse problem, a general formulation provided by *Singular Value Decomposition* (SVD) was introduced by Veronesi and Maynard [1]. The applicability of the SVD was subsequently investigated by a number of authors [2–6] and recent approaches have seen based on expressing the field at a number of discrete points in terms of the discrete points of the source distribution. In particular, the SVD can give an insight into the spatial resolution of the reconstructed source strength [6–8].

The work presented in Refs. [4–8] shows that the ill-conditioning of the matrix to be inverted can very often result in an ill-posed problem and this can be interpreted in terms of the small singular values which often specify the high spatial frequencies in the acoustic source distribution. However, in Refs. [7–9], particular conditions have been shown to lead to the acoustical inverse problem becoming optimally conditioned. These involve measurements undertaken in the near field as close as possible to the source or arranging the source and farfield data in a manner that results in the discrete farfield data and the source distribution constituting a *Discrete Fourier Transform* (DFT) relationship. The DFT relationship has the least sensitivity to errors of various kinds. Therefore, imaging from farfield measurements may be assisted greatly by the adoption of these optimally spaced sensors and sources.

However, in real-world applications, it sometimes is not so easy to realise the DFT relationship. Otherwise, when the sensor array is placed close to the source surface, the acoustic pressures at measurement positions may be modified by scattering, reflection or resonance caused by the small gap between the source surface and the sensor array. Furthermore, contamination of various kinds of errors in the measurements is inevitable. In such cases, in spite of the optimal arrangements of the sensors and sources, acoustical inverse problems often become ill-posed. Therefore, numerical procedures, which are called *regularisation*, are often imposed to produce reasonable solutions to the discrete ill-posed problems [4,6,8,10–14]. In such cases, the success of regularisation depends on the appropriate choice of the regularisation parameter. But, it is very difficult to determine the proper amount of regularisation without prior knowledge of either the acoustic sources or the contaminating measurement noise. Due to this difficulty, two methods, *Generalised Cross Validation* (GCV) [15–17] and the *L-curve method* [18–20], have been introduced. Neither of these methods requires prior information of either the source distribution to be reconstructed or the contaminating errors.

However, as shown in Refs. [7,8], the regularisation process may affect the spatial resolution of source reconstruction since the regularisation process also is closely connected with the small singular values associated with high spatial frequencies in the source distribution. Hence, useful information about the acoustic sources can be well resolved when the degree of the regularisation is appropriately determined. In other words, if excessive regularisation is imposed then both

resolution and estimation accuracy are considerably decreased. Therefore, it is important to be able to choose the right degree of regularisation when constructing an optimal estimate of the acoustic source distribution. However, clear guidelines for the right choice of regularisation parameter-determination methods have not yet been provided in dealing with acoustical inverse problems.

In this paper, the basic formulation of Tikhonov regularisation [21,22] is firstly described and an attempt is made to connect the use of the SVD to the regularisation process including the determination of regularisation parameters. In order to investigate the effect of the degree of regularisation on spatial resolution and accuracy, this paper presents an evaluation of the relative merits of GCV and the *L*-curve method. The abilities of the methods are illustrated when a range of inverse sound radiation problems are treated using well-known Tikhonov regularisation. This is investigated by exploring the relationship between estimation accuracy, noise level, and source and sensor geometry. This will enable practical guidelines to be proposed for determining the optimal regularisation parameter that is capable of producing the best possible spatial resolution of acoustic sources. Finally, some experimental results are presented when a volume velocity source distribution is reconstructed from farfield data with regularisation parameters provided by the two different methods.

2. Least-squares estimation and Tikhonov regularisation

2.1. Simple least-squares estimation

When a real source is modelled by N discrete acoustic sources, acoustic pressures measured at the same number of discrete field points as the modelled sources can be represented by using a frequency response function matrix $\mathbf{G}$ relating the model acoustic pressures $\mathbf{p}$ to the model complex source strengths $\mathbf{q}$. However, in practice contaminating errors of various kinds are inevitable. These errors include noise due to measurement contamination of complex acoustic pressures and errors involved in the model representation of the real acoustic source distribution. Hence, it is assumed that the difference between the model pressure $\mathbf{p}$ and the measured pressures $\hat{\mathbf{p}}$ can be expressed as the vector of complex errors given by $\mathbf{e} = \hat{\mathbf{p}} - \mathbf{p}$. Therefore, the measured acoustic pressures $\hat{\mathbf{p}}$ at the discrete field points can be expressed by

$$\hat{\mathbf{p}} = \mathbf{G}\mathbf{q} + \mathbf{e}, \tag{1}$$

where $\hat{\mathbf{p}}$ denotes the N-dimensional complex vector of the measured acoustic pressures and $\mathbf{q}$ represents the N-dimensional complex vector of the acoustic source strengths assumed. The estimate of the model source strength vector $\mathbf{q}$ is deduced by minimising the error criterion is defined by

$$J = \|\mathbf{e}\|^2 = \|\mathbf{G}\mathbf{q} - \hat{\mathbf{p}}\|^2, \tag{2}$$

where $\|\,\|$ denotes the 2-norm. The least-squares estimation of the acoustic source strengths $\mathbf{q}$ is given by [4–8]

$$\mathbf{q} = \mathbf{G}^{-1}\hat{\mathbf{p}}, \tag{3}$$

where the matrix $\mathbf{G}$ is assumed to be square.

In many practical cases, there is no unique solution to this equation, even if a solution exists, due to the presence of very small elements (i.e., singular or nearly singular values) in the matrix **G** to be inverted. It is, therefore, very useful to introduce the SVD which enables the complex matrix **G** to be decomposed into the following product of the three matrices [23]:

$$\mathbf{G} = \mathbf{U}\Sigma\mathbf{V}^{\mathrm{H}} = \sum_{i=1}^{N} \mathbf{u}_i \sigma_i \mathbf{v}_i^{\mathrm{H}}. \tag{4}$$

The matrix **U** is a matrix of left singular vectors $\mathbf{u}_i$ of the matrix **G**, and the matrix **V** is a matrix of right singular vectors $\mathbf{v}_i$ of the matrix **G**. Both matrices **U** and **V** are unitary and have the properties $\mathbf{U}^{\mathrm{H}} = \mathbf{U}^{-1}$ and $\mathbf{V}^{\mathrm{H}} = \mathbf{V}^{-1}$. Superscript H denotes Hermitian transpose. The $N \times N$ matrix Σ is given by

$$\Sigma = \begin{bmatrix} \sigma_1 & 0 & \cdots & 0 & 0 \\ 0 & \sigma_2 & \cdots & 0 & 0 \\ \vdots & \vdots & \vdots & \vdots & \vdots \\ 0 & 0 & \cdots & \sigma_{N-1} & 0 \\ 0 & 0 & \cdots & 0 & \sigma_N \end{bmatrix}, \tag{5}$$

where the matrix Σ is diagonal with elements σ_i which comprise the singular values of the matrix **G** (i.e., $\sigma_1 \geqslant \sigma_2 \geqslant \cdots \geqslant \sigma_N \geqslant 0$).

Substituting the transformed Eq. (4) provided by the SVD, and by using the orthonormal properties of the unitary matrices **U** and **V**, the least-squares estimation of the acoustic source strength can be written as

$$\mathbf{q} = \mathbf{V}\Sigma^{-1}\mathbf{U}^{\mathrm{H}}\hat{\mathbf{p}} = \sum_{i=1}^{N} \frac{\mathbf{u}_i^{\mathrm{H}}\hat{\mathbf{p}}}{\sigma_i}\mathbf{v}_i, \tag{6}$$

where the matrix Σ^{-1} is the inverse of the matrix Σ and is given by

$$\Sigma^{-1} = \begin{bmatrix} 1/\sigma_1 & 0 & \cdots & 0 & 0 \\ 0 & 1/\sigma_2 & \cdots & 0 & 0 \\ \vdots & \vdots & \vdots & \vdots & \vdots \\ 0 & 0 & \cdots & 1/\sigma_{N-1} & 0 \\ 0 & 0 & \cdots & 0 & 1/\sigma_N \end{bmatrix}. \tag{7}$$

As can be seen from Eqs. (5) and (7), the very small singular values (compared to the largest singular value σ_1) of the matrix Σ to be inverted will produce large quantities of elements in the matrix Σ^{-1}. This effect can introduce large errors into the solution given by Eq. (6). For example, if the magnitude of $|\mathbf{u}_i^{\mathrm{H}}\hat{\mathbf{p}}|$ is much greater than the associated singular value σ_i in Eq. (6), the reconstructed source strengths **q** will be dominated by the terms in the sum corresponding to the smallest singular value. Hence, as shown in Refs. [6–8,12,13], due to this behaviour of the small singular values of the matrix **G**, successful reconstruction of the acoustic source distribution cannot always be guaranteed by using only the simple least-squares method.

Therefore, in such cases, most numerical methods seek to overcome a problem with very small singular values in the matrix **G** by replacing the problem with a *nearby* well-conditioned problem

whose solution is a more satisfactory solution than the simple least-squares solution. It is thus important to appreciate that even when an inverse problem may be ill-conditioned, a useful solution can still be found by using regularisation.

2.2. Tikhonov regularisation

Briefly, the underlying idea of Tikhonov regularisation is that a regularised solution having a suitably small residual norm and satisfying additional constraints will be not too far from the desired, unknown solution. The general form of the error criterion between the true and the estimated solution can be defined as a weighted linear combination of a squared residual norm and the additional constraint. This is given by [21,22]

$$J = \|\mathbf{G}\mathbf{q} - \hat{\mathbf{p}}\|^2 + \beta\|\mathbf{L}\mathbf{q}\|^2 \tag{8}$$

where the regularisation parameter β controls the weight given to minimisation of the additional constraint $\|\mathbf{L}\mathbf{q}\|$ relative to minimisation of the residual norm $\|\mathbf{G}\mathbf{q} - \hat{\mathbf{p}}\|$.

In Eq. (8), when the non-negative definite matrix $\mathbf{L}$ is assumed to be the identity matrix $\mathbf{I}$ and the matrix $\mathbf{G}$ is assumed to be square matrix ($N \times N$), it is easy to show [24,25] that the acoustic source strength $\mathbf{q}_R$ can be deduced by minimising the error criterion J. The solution that minimises this error criterion is given by

$$\mathbf{q}_R = \mathbf{V}\Sigma_R^{-1}\mathbf{U}^{\mathrm{H}}\hat{\mathbf{p}} = \sum_{i=1}^{N}\left(\frac{\sigma_i^2}{\sigma_i^2 + \beta}\right)\frac{\mathbf{u}_i^{\mathrm{H}}\hat{\mathbf{p}}}{\sigma_i}\mathbf{v}_i, \tag{9}$$

where subscript R represents the regularised solution and β denotes the chosen regularisation parameter. The matrix Σ_R^{-1} is given by

$$\Sigma_R^{-1} = \begin{bmatrix} \sigma_1/(\sigma_1^2 + \beta) & 0 & \cdots & 0 \\ 0 & \sigma_2/(\sigma_2^2 + \beta) & \cdots & 0 \\ \vdots & \vdots & \vdots & \vdots \\ 0 & 0 & \cdots & \sigma_N/(\sigma_N^2 + \beta) \end{bmatrix}. \tag{10}$$

In Eq. (9), the *regularisation factor* R_f $(= \sigma_i^2/(\sigma_i^2 + \beta))$ has a close connection to the magnitude of $|\mathbf{u}_i^{\mathrm{H}}\hat{\mathbf{p}}/\sigma_i|$ and thus prevents the inversion of very small singular values from giving very large terms in the matrix Σ_R^{-1}. Therefore, the value of β should be chosen with care since it controls the properties of the regularised solution. For example, if too much regularisation is imposed, the result of the reconstruction will not fit the measured complex pressure data properly. On the other hand, if too little regularisation is used, it will be dominated by the contributions from various types of errors. Hence, the efficiency of the Tikhonov regularisation method is highly dependent on the proper choice of the regularisation parameter β that produces a fair balance between the perturbation error and the regularisation error [6,12–14].

3. Regularisation parameter-determination methods

3.1. Generalised cross validation and the L-curve method

Briefly, Generalised Cross Validation (GCV) seeks to strike an optimal balance between perturbation errors and regularisation errors for all valid regularisation parameters. The basis of the method is that the value of β_{GCV} is sought that minimises the Generalised Cross Validation function (GCV function) given by

$$GCV(\beta) = (1/N)\|\{\mathbf{I} - \mathbf{B}(\beta)\}\hat{\mathbf{p}}\|^2/[(1/N)\mathrm{Tr}\{\mathbf{I} - \mathbf{B}(\beta)\}]^2. \tag{11}$$

Full details of the derivation of this GCV function are presented in Refs. [4,8]. In Eq. (11), N denotes the number of measurement positions, Tr denotes the trace (sum of diagonal elements) of a matrix and $\mathbf{B}(\beta)$ denotes the influence matrix defined by $\mathbf{B}(\beta) = \mathbf{G}(\mathbf{G}^{\mathrm{H}}\mathbf{G} + \beta\mathbf{I})^{-1}\mathbf{G}^{\mathrm{H}}$ [4].

The denominator in Eq. (11) evaluates the perturbation errors caused by regularisation with the addition of β to the error criterion J. Thus, the denominator will become progressively smaller than unity and will tend to increase $GCV(\beta)$ as β is increased. The numerator represents the squared sum of residuals of the regularised solution. Hence, the GCV function evaluates both the errors in the solution and the inaccuracy introduced into the matrix $\mathbf{G}$ to be inverted by the inclusion of the regularisation parameter chosen. Thus, the regularisation parameter for the regularised solution $\mathbf{q}_R$ in Eq. (9) is determined by minimising the above GCV function. Fig. 1 shows a typical form of the GCV function and a diagrammatic representation of the regularisation parameter β_{GCV} provided by GCV. Successful applications of GCV to acoustical inverse problems have been demonstrated in Refs. [4–8,12–14].

Another convenient tool for determining the appropriate regularisation parameters without prior knowledge is the so-called the L-curve method. The method is a graphical tool with a plot of the regularised solution against its residual for all valid regularisation parameters. In other words, the L-curve is a plot of the norm $\|\mathbf{Lq}\|$ of the regularised solution versus the corresponding residual norm $\|\mathbf{Gq} - \hat{\mathbf{p}}\|$ for all valid regularisation parameters. The principle is based on the fact that there is a distinct corner which separates the vertical and the horizontal parts of the curve, when these two quantities are plotted on a log–log scale, as depicted in Fig. 2. The vertical part of

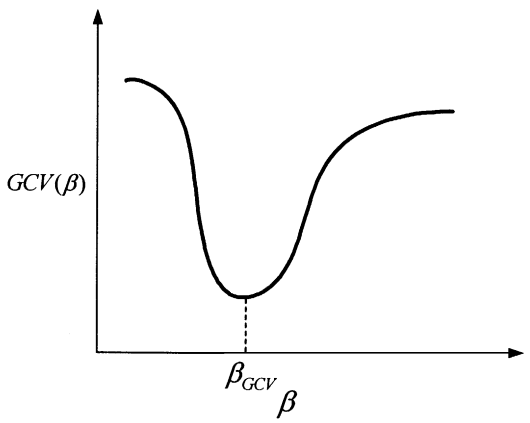

Fig. 1. A typical form of the GCV function.

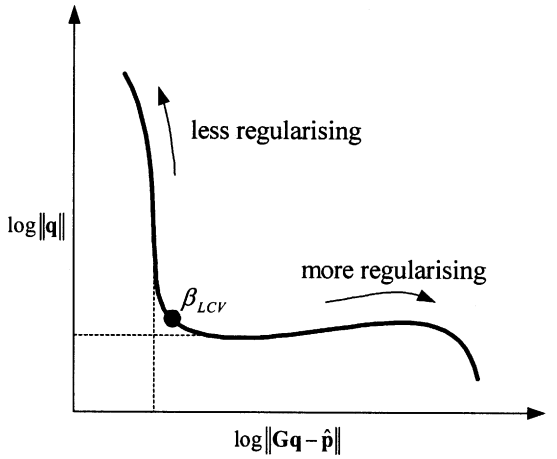

Fig. 2. The generic form of the L-curve [18].

the L-curve corresponds to perturbations of the regularised solution resulting from contamination errors, and the horizontal part represents small changes of the regularised solution caused by regularisation errors [18]. In other words, the horizontal part corresponds to solutions where the regularisation parameter is too large and the solution is dominated by regularisation errors. The vertical part corresponds to solutions where the regularisation parameter is too small and the solution is dominated by contaminating errors magnified by the division by small singular values during the inversion process. Therefore, the idea of the L-curve criterion for choosing the regularisation parameter is to determine a point on this curve that is at the "corner" of the vertical piece as illustrated in Fig. 2.

A computable formula has been suggested for choosing the corner on the L-curve where the curvature is maximum. This is described in Ref. [20]. Therefore, if the L-curve is twice continuously differentiable, then it can be straightforward to compute the curvature $L(\beta)$ of the L-curve by means of the formula [20]

$$L(\beta) = (\tilde{\rho}'\tilde{\eta}'' - \tilde{\rho}''\tilde{\eta}')/((\tilde{\rho}')^2 + (\tilde{\eta}')^2)^{3/2}, \tag{12}$$

where $\eta = \|\mathbf{q}_R\|^2, \rho = \|\mathbf{G}\mathbf{q}_R - \hat{\mathbf{p}}\|^2$. Also $\tilde{\eta} = \log\eta$, $\tilde{\rho} = \log\rho$ and the prime denotes differentiation with respect to the regularisation parameter β. The appropriate regularisation parameter β_{LCV} provided by the L-curve method corresponds to the maximum curvature of the L-shaped appearance. Details of practical applications and calculation tools for the L-curve method have been presented in Refs. [18–20,26–28].

3.2. An illustrative three-dimensional simulation

In order to demonstrate how the regularisation parameter-determination methods work, some simulated results are presented of an acoustical radiation problem with the sensor and source geometry depicted in Fig. 3. This geometry models a planar vibrating surface radiating in an acoustic field. Here, the planar vibrating surface is modelled as a family of point monopole sources and the equivalent number of sensors in the field is assumed to sense acoustic pressures

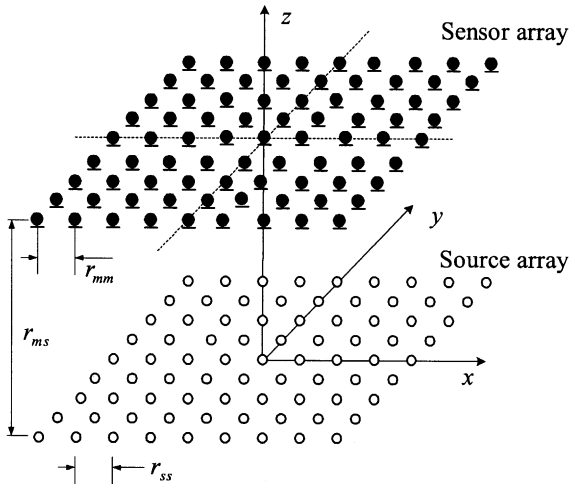

Fig. 3. The planar type sensor and source geometry (9×9 sensors and sources).

(here, 9×9 sensors and sources have been used). Note that measurement errors, which are simulated by running 500 random trials, were added to the pressure field data. The inter-sensor spacing r_{mm} is adjusted to be equal to the inter-source spacing r_{ss} and the sensor array plane is r_{ms} away from the source array plane. The Green function defining the frequency response relationship between the acoustic pressure and the associated acoustic source distribution can be written as

$$\mathrm{G}(kr) = (\mathrm{j}\omega\rho_0/2\pi r)\,\mathrm{e}^{-\mathrm{j}kr}, \tag{13}$$

where ρ_0 is the density, k is the wavenumber ($k = \omega/c_0$ where ω is the angular frequency and c_0 is the sound speed) and r denotes the distance from a source to a field point.

In order to evaluate the effectiveness of GCV and the L-curve, when detailed source strengths to be reconstructed are assumed to be known (here, simply only one point monopole source located at the centre of the planar source array is assumed to have unit strength), the mean squared error (MSE) between the known and regularised source strengths for all valid regularisation parameters is used. Thus, the regularisation parameter β_{MSE} derived from the estimation of MSE corresponds to the minimum of the MSE function. This is given by [7,8]

$$\beta_{MSE} = \min_{\beta}\,[MSE(\beta)] = \min_{\beta}\,[E[(\mathbf{q}_R - \mathbf{q}_T)^{\mathrm{H}}(\mathbf{q}_R - \mathbf{q}_T)]], \tag{14}$$

where $\mathbf{q}_T$ represents the vector of the true source strengths which are assumed here to be known.

In Fig. 4(a), firstly, it can be found that two regularisation parameter-determination methods offer reasonable regularisation parameters based on comparison of magnitudes of β_{GCV} and β_{LCV} with the magnitude of β_{MSE} for a randomly selected acoustical condition. It is clearly evident from Fig. 4(b) that the magnitude variation of $|\mathbf{u}_i^{\mathrm{H}}\hat{\mathbf{p}}|$ is properly suppressed by the chosen regularisation parameters, β_{GCV} and β_{LCV}, compared to that from the simple least-squares method (i.e., without regularisation; when $\beta = 0$). For example, Figs. 4(c) and (d) show good reconstruction results produced by using Tikhonov regularisation with β_{GCV} and β_{LCV}. The results for the other acoustical conditions selected are shown in Figs. 5 and 6. These show that the regularisation

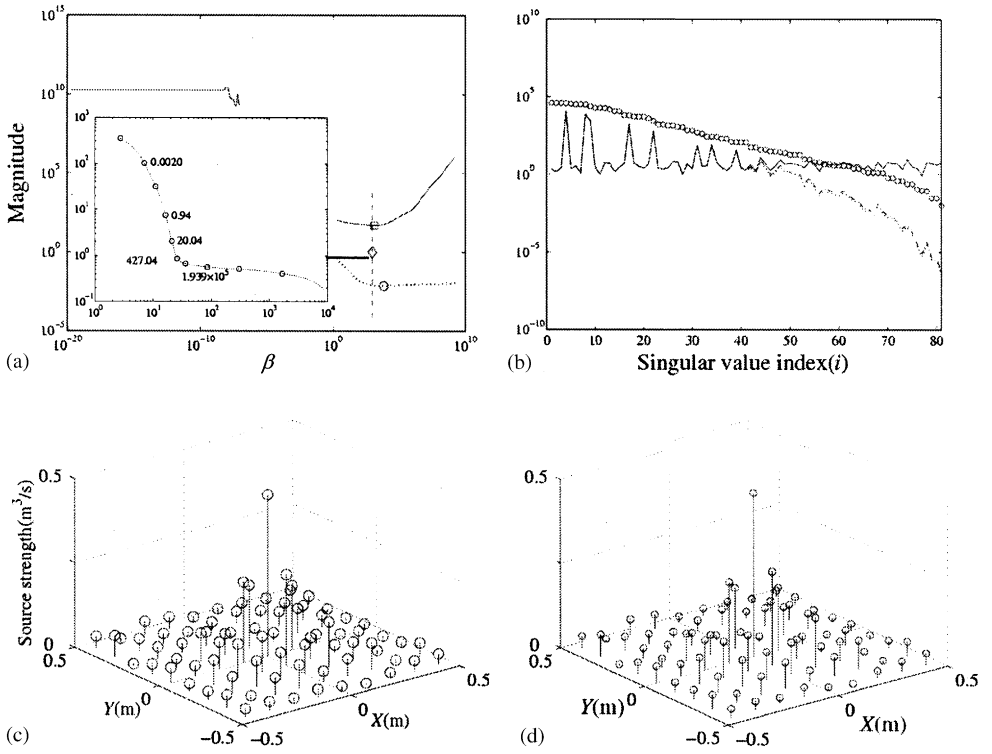

Fig. 4. Results of the reconstruction for the geometry Fig. 3 with only a single source present when $r_{ss}/\lambda = 0.25$, $r_{ms} = \lambda$ and adding 20% measurement noise: (a) comparison between β_{MSE} (○), β_{GCV} (□) and β_{LCV} (◇); (b) the magnitude variation of σ_i (circle) and $R_f|\mathbf{u}_i^{\mathrm{H}}\hat{\mathbf{p}}|$ at $\beta = 0$ (solid line), $\beta = \beta_{GCV}$ (dotted line) and $\beta = \beta_{LCV}$ (dashed line); (c) reconstructed result when $\beta = \beta_{GCV}$; (d) reconstructed result when $\beta = \beta_{LCV}$.

parameters determined by the two methods still work properly to prevent the "blow-up" in reconstruction caused by the inversion of very small singular values. Reasonable solutions are thus produced. It can be also clearly seen that there is good agreement between values for β_{GCV}, β_{LCV} and β_{MSE}.

In the simulated results shown, both methods seem to work well in determining the optimal amount of regularisation. However, it should be mentioned that both methods do not always produce satisfactory results. For example, the *L*-curve method often is not convergent under certain conditions [29,30], i.e., when the magnitude of $|\mathbf{u}_i^{\mathrm{H}}\hat{\mathbf{p}}|$ decays at the same rate or less rapidly than the associated singular values. Moreover, when the frequency response function matrix $\mathbf{G}$ to be inverted is relatively well-conditioned, the distinct corner corresponding to the maximum curvature of the *L*-curve often cannot be seen clearly [4]. On the other hand, in the case demonstrated in Refs. [27,28], the *L*-curve method can be a better choice for determining the proper regularisation parameters than GCV. Furthermore, GCV is likely to fail to provide an optimal regularisation parameter if errors contaminating the measured data are highly correlated [17] and some empirical evidence of the possibility has been presented [31]. Also, in some practical cases for acoustical inverse problems, it has been demonstrated [6,7] that the minima of the GCV

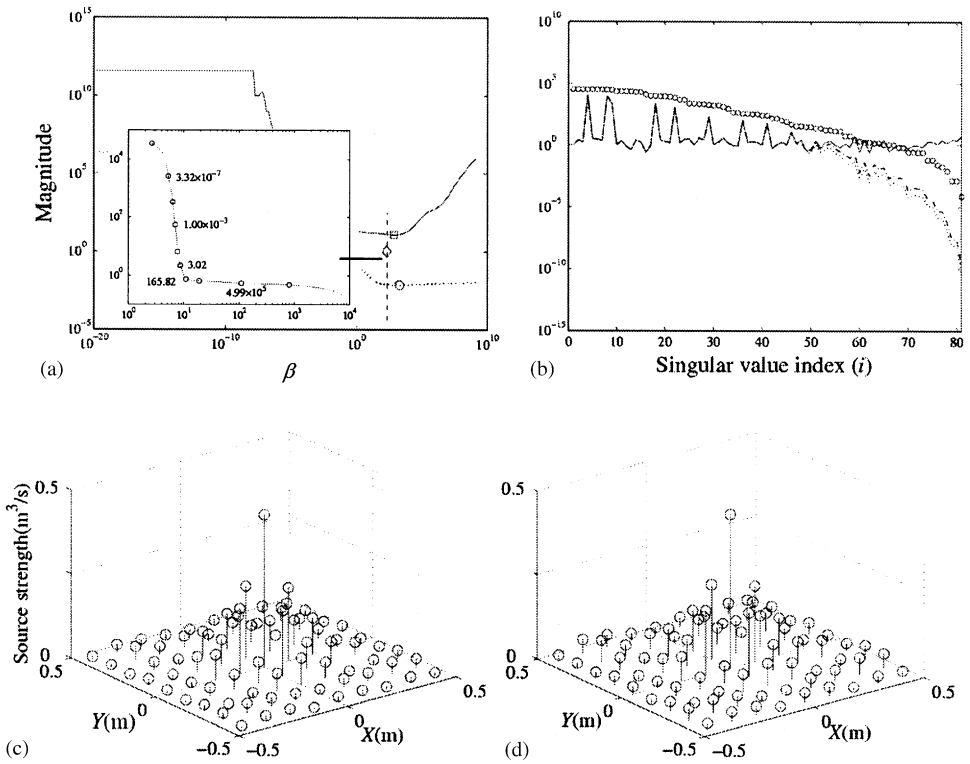

Fig. 5. Results of the reconstruction for the geometry Fig. 3 with only a single source present when $r_{ss}/\lambda = 0.5$, $r_{ms} = 5\lambda$ and adding 20% measurement noise: (a) comparison between β_{MSE} (○), β_{GCV} (□) and β_{LCV} (◇); (b) the magnitude variation of σ_i (circle) and $R_f|\mathbf{u}_i^{\mathrm{H}}\hat{\mathbf{p}}|$ at $\beta = 0$ (solid line), $\beta = \beta_{GCV}$ (dotted line) and $\beta = \beta_{LCV}$ (dashed line); (c) reconstructed result when $\beta = \beta_{GCV}$; (d) reconstructed result when $\beta = \beta_{LCV}$.

functions are not exhibited clearly since the GCV function has a broad flat minimum over a certain range of valid regularisation parameters.

Hence, in practice, the determination of the proper choice of the regularisation parameter seems not to be completely straightforward and furthermore there is no universally accepted method. Therefore, in order to obtain the best possible estimate of the underlying and the unknown solution, it will be valuable to compare the abilities of these two well-known regularisation parameter-determination strategies for a wide range of acoustic conditions. The simulated results presented in the following section may provide useful guidelines.

3.3. Performance comparisons of two regularisation parameter-determination methods

As demonstrated in the previous section, it is clear that the key to producing fine spatial resolution information of acoustic sources is an effective method for determining the right amount of regularisation. The section will explore the relationships between estimated accuracy and spatial resolution, noise-level and source/sensor geometry, when a range of inverse sound radiation problems is treated using Tikhonov regularisation.

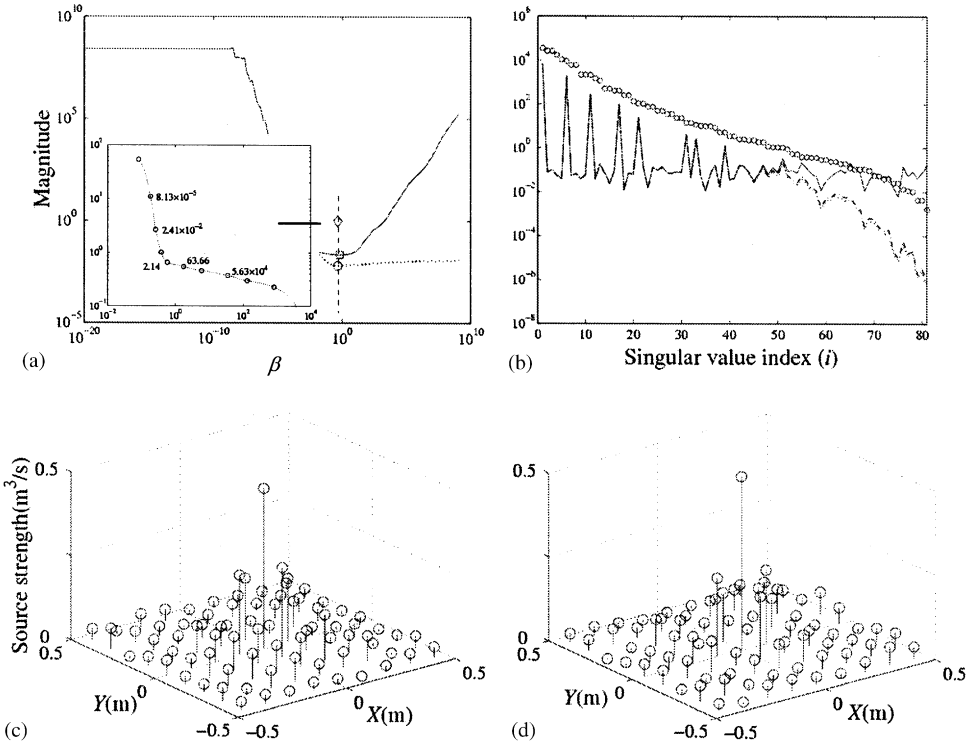

Fig. 6. Results of the reconstruction for the geometry Fig. 3 with only a single source present when $r_{ss}/\lambda = 0.125$, $r_{ms} = 0.5\lambda$ and adding 20% measurement noise: (a) comparison between β_{MSE} (○), β_{GCV} (□) and β_{LCV} (◇); (b) the magnitude variation of σ_i (circle) and $R_f|\mathbf{u}_i^{\mathrm{H}}\hat{\mathbf{p}}|$ at $\beta = 0$ (solid line), $\beta = \beta_{GCV}$ (dotted line) and $\beta = \beta_{LCV}$ (dashed line); (c) reconstructed result when $\beta = \beta_{GCV}$; (d) reconstructed result when $\beta = \beta_{LCV}$.

For the investigation the planar sensor and source array depicted in Fig. 3 has again been used with the same acoustical conditions, including the Green function described in the previous section. In addition, a hemispherical sensor array has also been used as an optimal sensor array as suggested in Refs. [7–9]. This attempt can make the connection between contaminating errors and the abilities of the two regularisation parameter-determination methods, since the acoustical inverse problem with the hemispherical sensor array becomes extremely well-conditioned at certain frequencies.

Firstly, in order to investigate the efficiencies of the methods in determining regularisation parameters in conjunction with singular value distribution of the matrix $\mathbf{G}$, it is necessary to observe the behaviour of the condition number $\kappa(\mathbf{G})$ of the matrix. Here, the condition number $\kappa(\mathbf{G})$ is widely employed as the most important attribute of the matrix $\mathbf{G}$ relating the behaviour of the small singular values, and is defined by the ratio between the largest and the smallest non-zero singular values [23]. Fig. 7 shows variations of the condition number $\kappa(\mathbf{G})$ for the planar sensor array and the hemispherical sensor array with respect to the geometrical arrangement of sensors and sources (i.e., non-dimensional source spacing r_{ss}/λ and non-dimensional distance r_{ms}/r_{ss} between the sensor array and the source array). As the planar sensor array is placed in the field

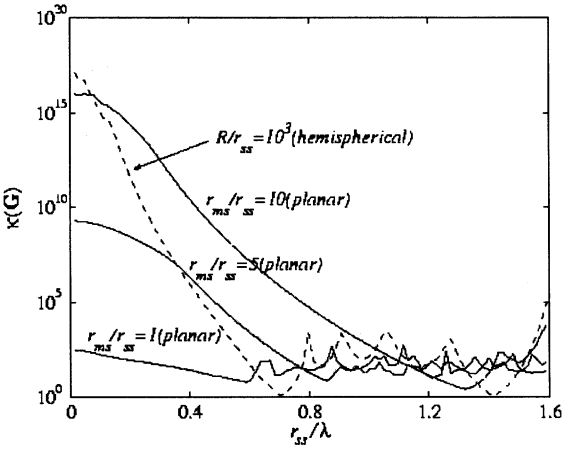

Fig. 7. Variations of condition number for the planar and the hemispherical sensor array (9×9 sensors and sources).

close to the source surface, it can be clearly seen that the conditioning of the matrix $\mathbf{G}$ can be much improved over the whole range of r_{ss}/λ. However, as the non-dimensional distance r_{ms}/r_{ss} increases, the acoustical inverse problem becomes ill-conditioned, particularly in the region of small r_{ss}/λ. Meanwhile, in the case with the hemispherical sensor array (which has the same number of sensors as the planar sensor array) in the farfield (for example, when the sensors are located on the hemisphere with radius R where $R = 10^3 r_{ss}$), the problem becomes best conditioned when $r_{ss}/\lambda = 1/\sqrt{2}$ and $2/\sqrt{2}$. In this case, the matrix $\mathbf{G}$ has unit condition number and thus the reconstructed solution will be due to only the contaminating errors without magnification by the inversion process.

In order to evaluate the performances of the two methods, the regularisation parameters, β_{GCV} and β_{LCV}, respectively determined by GCV and the L-curve method, will be compared with β_{MSE} (which is given by Eq. (14)). This is undertaken for a wide range of acoustical conditions, non-dimensional source-spacing r_{ss}/λ where λ denotes the acoustic wavelength and level of noise contamination $E_r = |e|/|(\sqrt{\mathbf{p}^{\mathrm{H}}\mathbf{p}} - e)|$ where e is the amplitude of the assumed noise. Firstly, Figs. 8–10 show the magnitude variations of $|\Delta\beta_{GCV}|^{0.5}$ $(= |\beta_{GCV} - \beta_{MSE}|^{0.5})$ and $|\Delta\beta_{LCV}|^{0.5}$ $(= |\beta_{LCV} - \beta_{MSE}|^{0.5})$ for the planar sensor array over a wide range of non-dimensional source spacing r_{ss}/λ and signal to noise ratio E_r. Figs. 8(a) and (b) show the results when the planar sensor array is placed in the field close to the sources, for example when r_{ms} is equal to r_{ss} (i.e., the acoustical inverse problem becomes well-conditioned in the whole range of r_{ss}/λ as shown in Fig. 7). The magnitude of $|\Delta\beta_{GCV}|^{0.5}$ (i.e., the difference between β_{MSE} and β_{GCV}) is much smaller for the whole range of non-dimensional source spacing with a relatively low level of contaminating noise compared to that of $|\Delta\beta_{LCV}|^{0.5}$ (i.e., the difference between β_{MSE} and β_{LCV}). Contrary to this, in the region containing highly contaminating noise (i.e., when E_r is greater than about 0.1), the magnitude of $|\Delta\beta_{GCV}|^{0.5}$ tends to be larger than that of $|\Delta\beta_{LCV}|^{0.5}$, because GCV provides too small a regularisation parameter as illustrated in Fig. 8(c).

When the planar sensor array is deployed far from the sources, for example when r_{ms} equals to $5r_{ss}$ and $10r_{ss}$ as demonstrated in Figs. 9 and 10, the magnitude of $|\Delta\beta_{GCV}|^{0.5}$ is still much smaller in relatively low levels of contaminating noise for all values of r_{ss}/λ. However, similarly to the case

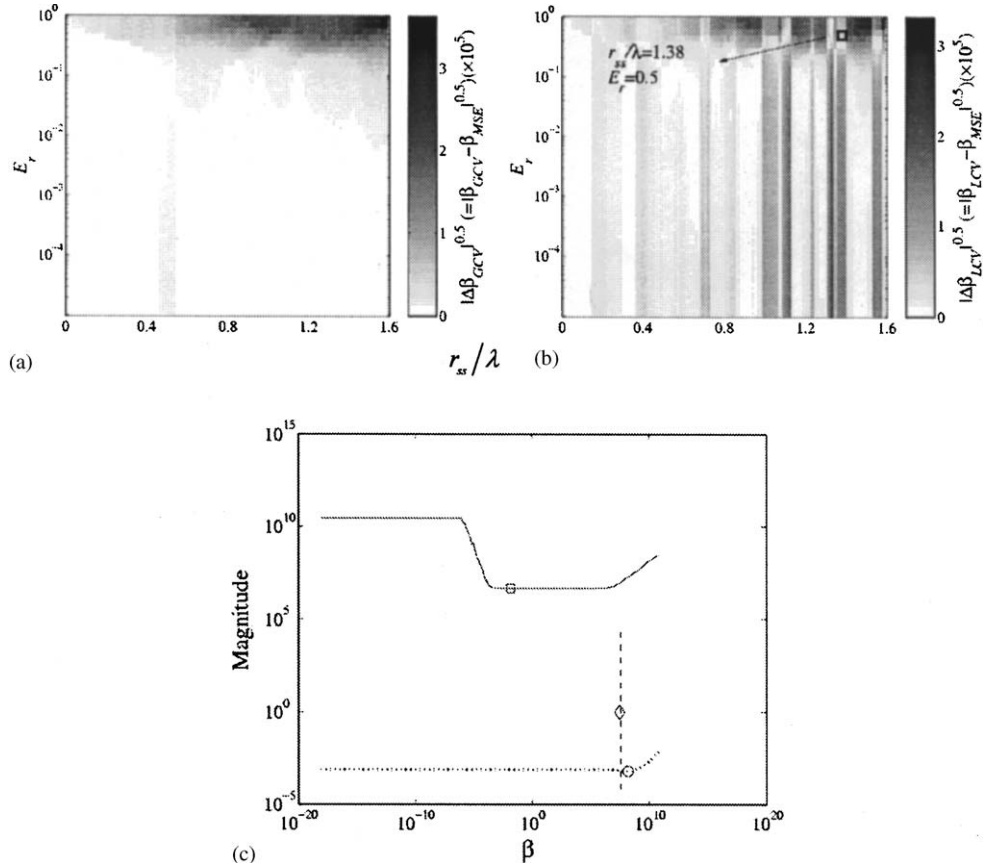

Fig. 8. Performance comparison of two regularisation parameter-determination methods for the planar sensor array (9×9 sensors and sources), when $r_{ms} = r_{ss}$: (a) variation of $|\Delta\beta_{GCV}|^{0.5}$ ($= |\beta_{GCV} - \beta_{MSE}|^{0.5}$); (b) variation of $|\Delta\beta_{LCV}|^{0.5}$ ($= |\beta_{LCV} - \beta_{MSE}|^{0.5}$); (c) comparison between β_{MSE} (○), β_{GCV} (□) and β_{LCV} (◇) when $r_{ss}/\lambda = 1.38$ and $E_r = 0.5$.

shown in Fig. 8, when problems have very small condition number $\kappa(\mathbf{G})$ and the measured acoustic pressures contain relatively high levels of noise, GCV calculates very small regularisation parameters as illustrated in Figs. 9(c) and 10(c).

Results are shown in Fig. 11 for the hemispherical sensor array in the farfield (when $R = 10^3 r_{ss}$ where the field points are located on the hemisphere of radius R). In this case, GCV still appears to be a better choice than the L-curve method at relatively low noise levels. When the problem becomes optimally conditioned (for example, when $r_{ss}/\lambda = 1/\sqrt{2}$ and $2/\sqrt{2}$) with relatively high noise contamination, the L-curve method can be better for determining the proper regularisation parameters since GCV provides too small a regularisation parameter compared with β_{LCV} as shown in Fig. 11(c). However, in the case shown in Fig. 11(d) (when $r_{ss}/\lambda = 1.2$, $E_r = 0.7$ and the problem becomes relatively ill-conditioned), GCV works well even in the same noise level as that of Fig. 11(c).

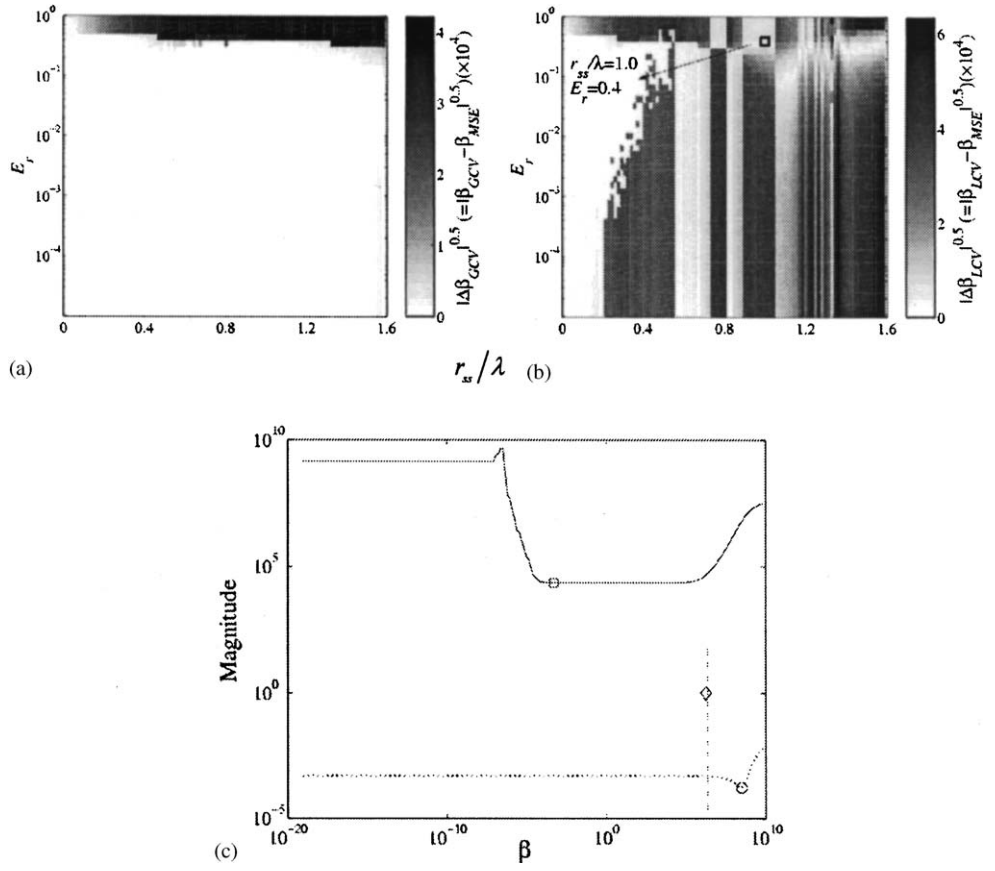

Fig. 9. Performance comparison of two regularisation parameter-determination methods for the planar sensor array (9×9 sensors and sources), when $r_{ms} = 5r_{ss}$: (a) variation of $|\Delta\beta_{GCV}|^{0.5}$ ($= |\beta_{GCV} - \beta_{MSE}|^{0.5}$); (b) variation of $|\Delta\beta_{LCV}|^{0.5}$ ($= |\beta_{LCV} - \beta_{MSE}|^{0.5}$); (c) comparison between β_{MSE} ($\bigcirc$), β_{GCV} ($\square$) and β_{LCV} ($\diamond$) when $r_{ss}/\lambda = 1.0$ and $E_r = 0.4$.

As a result of the numerical simulations presented in this section, the *L*-curve method seems to be effective particularly when the acoustical inverse problem becomes extremely well conditioned (i.e., when the solution of the problem is mainly dominated by errors, for example, or when the sensor array is placed in the field close to the sources or at a certain frequency with optimally spaced sensors). However, in practice, it is sometimes not so easy to realise the optimal sensor/source geometry for broadband acoustic sources or very high spatial frequencies. In such cases, GCV may be a better choice for the determination of the optimal amount of regularisation.

In addition, GCV works well particularly in acoustical conditions with a relatively low level of contaminating noise. In other words, it appears from the results that the regularisation parameter β_{GCV} deduced from GCV is always reasonably close to that for producing minimum mean squared error except at high noise levels ($E_r \geqslant 10^{-1}$). The *L*-curve method on other hand appears to give a more unpredictable variation from β_{MSE} when noise levels are low.

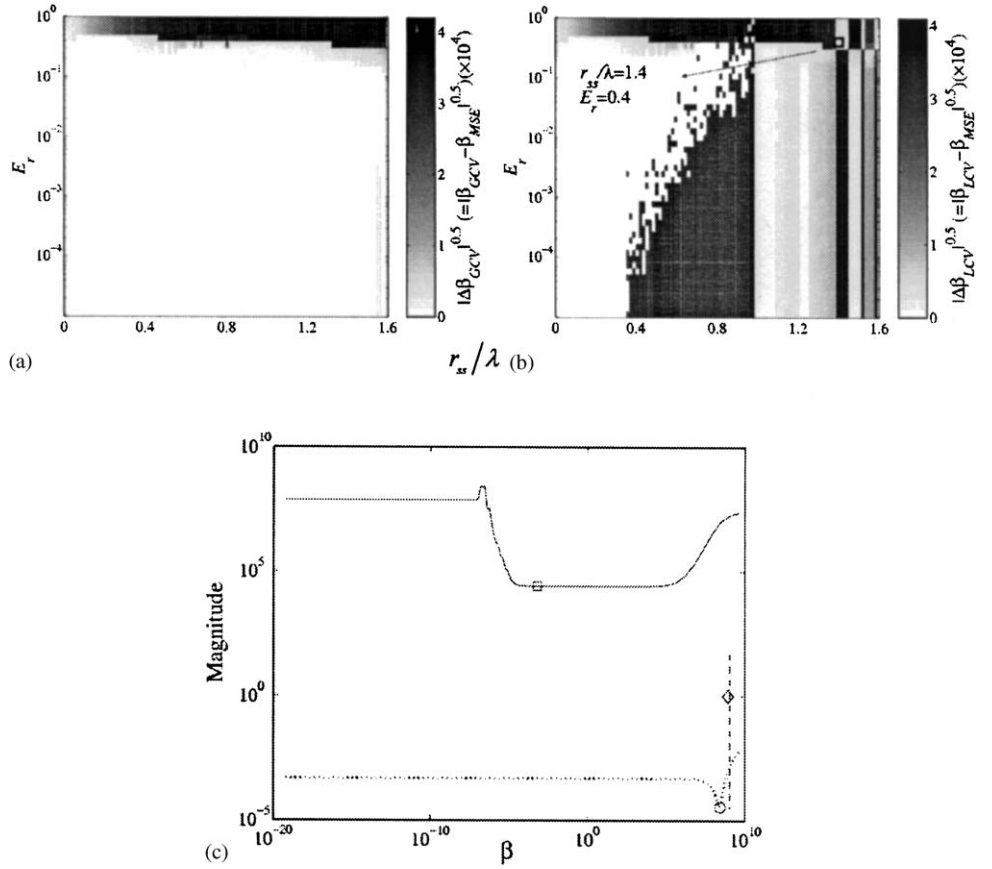

Fig. 10. Performance comparison of two regularisation parameter-determination methods for the planar sensor array (9×9 sensors and sources), when $r_{ms} = 10r_{ss}$: (a) variation of $|\Delta\beta_{GCV}|^{0.5}$ ($= |\beta_{GCV} - \beta_{MSE}|^{0.5}$); (b) variation of $|\Delta\beta_{LCV}|^{0.5}$ ($= |\beta_{LCV} - \beta_{MSE}|^{0.5}$); (c) comparison between β_{MSE} (○), β_{GCV} (□) and β_{LCV} (◇) when $r_{ss}/\lambda = 1.4$ and $E_r = 0.4$.

4. Experimental verification: reconstruction of volume velocity sources

4.1. Experimental system

Now one moves to a practical demonstration of the guidelines suggested and see how they work in an experimental application. Firstly, in this section, practical aspects of two regularisation parameter-determination methods will be related to the spatial resolution and the accuracy of reconstructed source images. The experimental validation to be presented consists of the reconstruction of a volume velocity source distribution with regularisation parameters provided by two different methods from measured farfield data. Subsequently, the capability of the hemispherical sensor array will be demonstrated experimentally and compared with that of the planar sensor array.

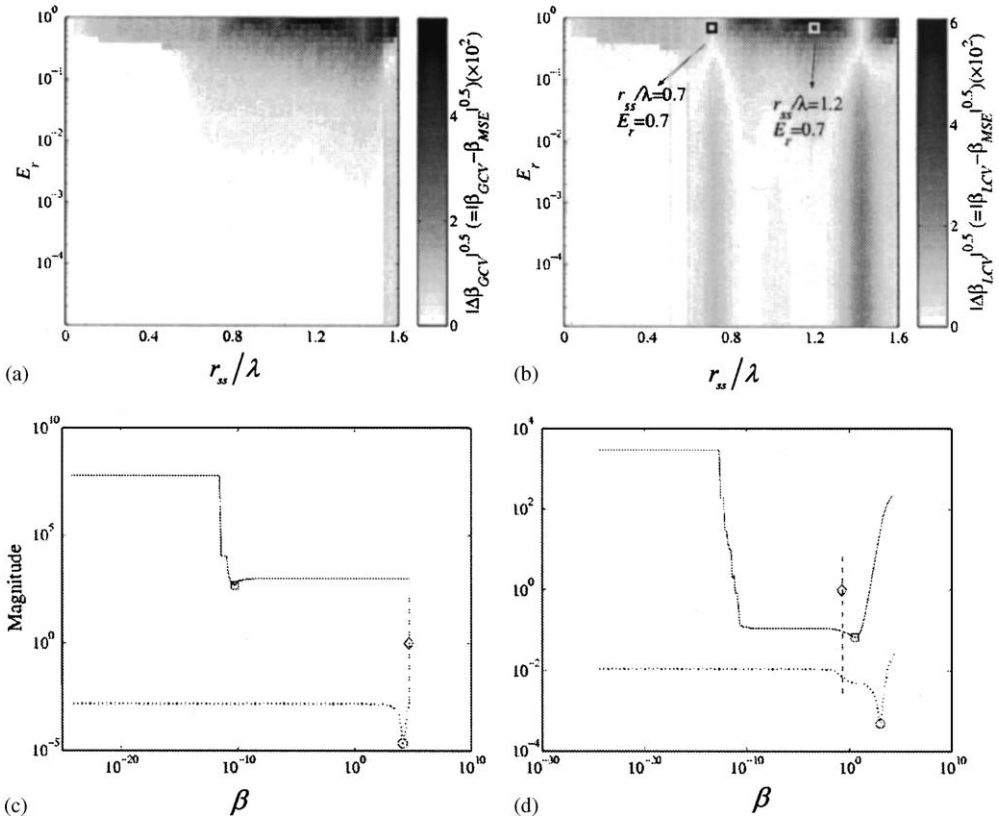

Fig. 11. Performance comparison of two regularisation parameter-determination methods for the hemispherical sensor array (9×9 sensors and sources), when $R = 10^3 r_{ss}$: (a) variation of $|\Delta\beta_{GCV}|^{0.5}$ ($= |\beta_{GCV} - \beta_{MSE}|^{0.5}$); (b) variation of $|\Delta\beta_{LCV}|^{0.5}$ ($= |\beta_{LCV} - \beta_{MSE}|^{0.5}$); (c) when $r_{ss}/\lambda = 0.7$ and $E_r = 0.7$; (d) when $r_{ss}/\lambda = 1.2$ and $E_r = 0.7$. Key for (c) and (d): ○, β_{MSE}; □, β_{GCV}; ◇, β_{LCV}.

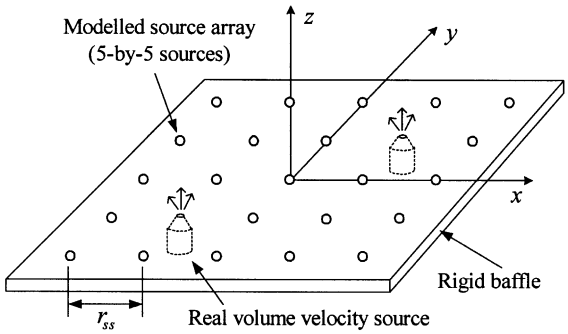

Fig. 12. A schematic diagram for the modelled sources.

A schematic representation of the real volume velocity sources and the source array used is illustrated in Fig. 12. Similarly to the geometrical arrangement of sources depicted in Fig. 3, a planar source array is modelled consisting of 5×5 volume velocity sources with the inter-source

spacing, $r_{ss} = 0.25$ m. Two real sources generate the acoustic field, where two small loudspeakers are mounted on the rear side of a rigid baffle. The details of the real sources, such as their locations and strengths, are assumed unknown, and thus it is assumed that there are 25 model sources. The loudspeakers are driven individually by completely different random signals. The source strength of each real source (for convenience, hereafter this is called "true source strength") was calibrated by the farfield acoustic pressure $\hat{p}(\omega)$ which is measured by the sensors at a known distance away from the sources. The true source strength is normalised by the simultaneously measured input voltage $V(\omega)$ which consisted of a white noise signal for driving the loudspeakers. This is obtained from

$$q(\omega)/V(\omega) = (1/\mathrm{G}(kr))\hat{p}(\omega)/V(\omega), \tag{15}$$

where the same Green function $\mathrm{G}(kr)$ as in Eq. (13) is used. The procedure is repeated for another volume velocity source. All experiments have been undertaken in the ISVR anechoic chamber with dimensions 9.15 m × 9.15 m × 7.32 m.

By using the experimental set-up shown in Fig. 13, farfield acoustic pressures at a planar (5 × 5 sensors) and a hemispherical sensor array (which has the same number of sensors as the planar sensor array) were simultaneously measured. Then, the measured data were stored in 64-channel digital tape recorder. In order to compare directly with the true source distribution in Eq. (15), all unknown source strengths to be reconstructed were also normalised by the simultaneously measured input voltages $V(\omega)$. The sensors on the hemisphere with radius R (= 2 m) were positioned with the two-dimensional discrete Fourier transform relationships between the measured farfield pressures and the source distribution. The full details of theoretical developments for this particular array have been presented in Refs. [7–9]. The 5 × 5 planar sensor array is the same distance 2 m with the radius of the hemispherical sensor array away from the source plane. The inter-sensor spacing r_{mm} was adjusted to be equal to the inter-source

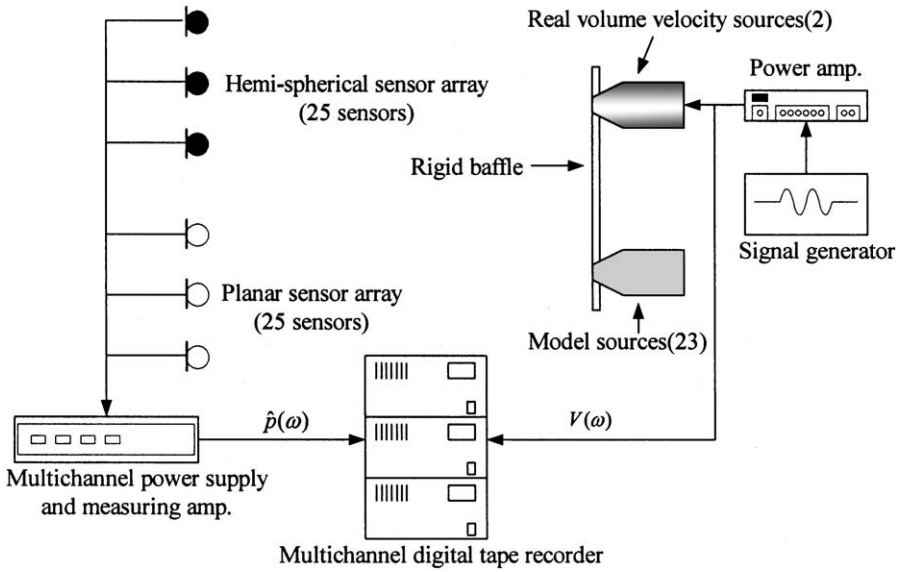

Fig. 13. A schematic diagram of the experimental set-up for measurements.

spacing, $r_{ss} = 0.25$ m. This is equivalent to the projected inter-sensor spacing to the source plane for the hemispherical sensor array.

4.2. Performance of regularisation parameter-determination methods

Measurements for experimental reconstruction of the volume velocity source distribution have been undertaken with the experimental models described in the previous section. In the experimental reconstruction process, the analytical Green function given by Eq. (13) has been used for frequency response relations between the farfield pressures and the source distribution. Firstly, Fig. 14 illustrates the condition number $\kappa(\mathbf{G})$ of the frequency response function matrices $\mathbf{G}$ for two experimental models. As shown in this figure, the experimental model with the hemispherical sensor array maintains better conditioning of the matrix $\mathbf{G}$ in the region of relatively small r_{ss}/λ. Furthermore, when the inter-source spacing $r_{ss} = \lambda/\sqrt{2}$, the problem becomes best conditioned and thus the sensor array has the least sensitivity to contaminating noise.

It is valuable to view the effectiveness of the two regularisation parameter-determination methods examined in Section 3 when they are applied to the experimental reconstruction process. Reconstruction results are compared under the same conditions which are produced with the two different types of sensor array (i.e., the planar and the hemispherical sensor array). Firstly, Fig. 15 shows mean squared errors (MSE) between the reconstructed source distribution produced by Tikhonov regularisation and the true source distribution measured directly, when only one real source generates an acoustic field out of a total of the 25 modelled sources depicted in Fig. 12. For the true source distribution, the strengths of the modelled sources are assumed to be equal to zero except for one real source. In this figure, it is clear that the accuracy of the reconstructed result for the real source is largely improved by Tikhonov regularisation with the regularisation parameters, β_{GCV} and β_{LCV}, compared with simple least-squares estimation (i.e., when $\beta = 0$; without regularisation). Furthermore, it can be seen that the optimally spaced sensors, for example here

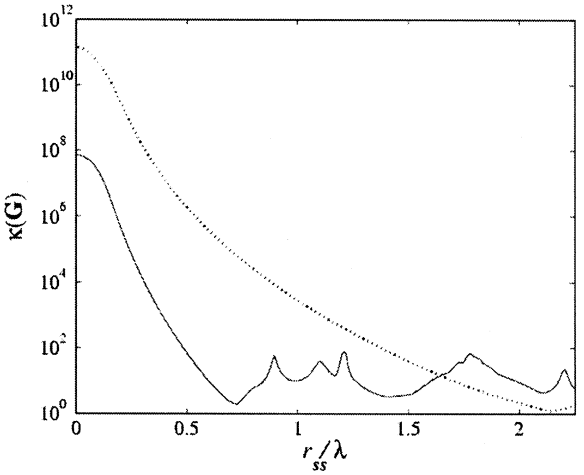

Fig. 14. Condition number variations of the frequency response function matrices for the experimental models: planar sensor array (dotted line), hemispherical sensor array (solid line).

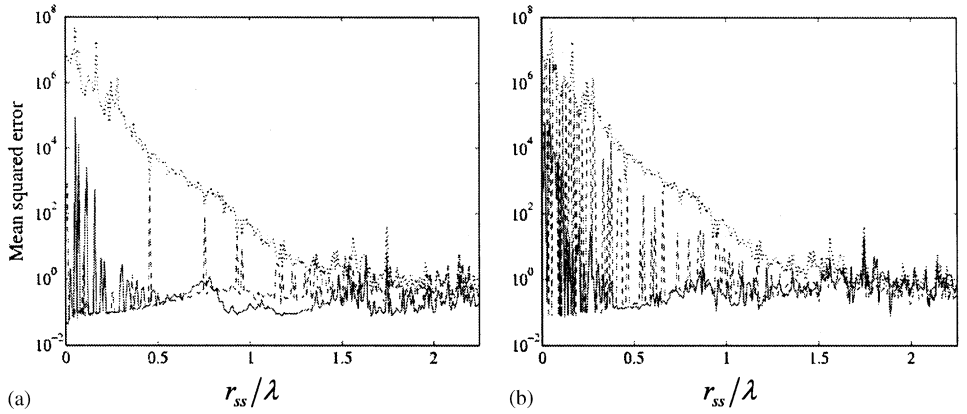

Fig. 15. Reconstructed source strengths produced by the two regularisation parameter-determination methods, when the radiated field is generated by only one real acoustic source for (a) Tikhonov regularisation with β_{GCV}: dotted line, planar sensor array ($\beta = 0$); dashed line, planar sensor array ($\beta = \beta_{GCV}$); solid line, hemispherical sensor array ($\beta = \beta_{GCE}$), and (b) Tikhonov regularisation with β_{LCV}: dotted line, planar sensor array ($\beta = 0$); dashed line, planar sensor array ($\beta = \beta_{LCV}$); solid line, hemispherical sensor array ($\beta = \beta_{LCV}$).

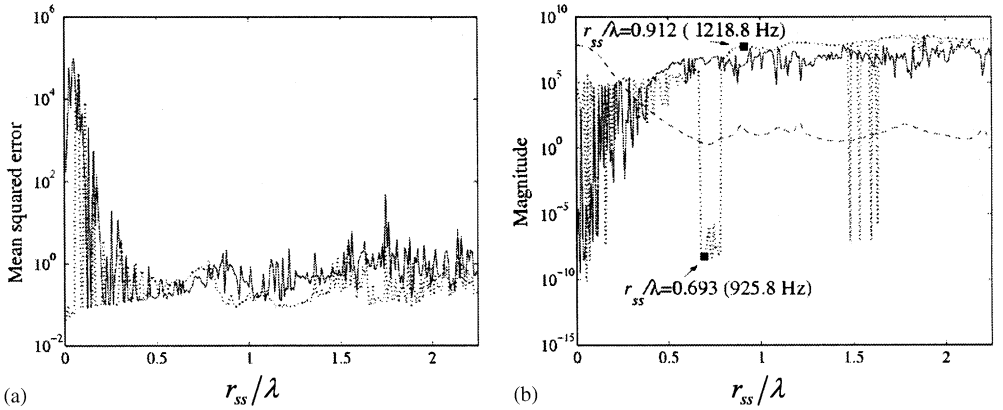

Fig. 16. Performance comparison of the two regularisation parameter-determination methods, when the radiated field, which is measured with the hemispherical sensor array, is generated by one real acoustic source: (a) mean squared errors produced by Tikhonov regularisation with GCV and the L-curve method (solid line, $\beta = \beta_{GCV}$; dotted line, $\beta = \beta_{LCV}$); (b) magnitude variations of the condition number and the regularisation parameters (solid line, $\beta = \beta_{GCV}$; dotted line, $\beta = \beta_{LCV}$; dashed line, $\kappa(\mathbf{G}_{\mathrm{H}})$).

the hemispherical type sensors, provide better resolution and accuracy of reconstructed source distribution particularly in the region of relatively small r_{ss}/λ.

In order to compare directly the abilities of the two regularisation parameter-determination methods considered here, mean squared errors of reconstructed source distribution produced by Tikhonov regularisation with β_{GCV} and β_{LCV} are shown in Fig. 16. The radiated sound field, which is measured with the hemispherical sensor array in the farfield, is generated by only one real acoustic source at an unknown position. In this case, GCV appears to give a better choice of regularisation parameter for reconstruction than the L-curve method since the mean squared

errors of the reconstructed source distribution with β_{GCV} are smaller over a wide range of non-dimensional source spacing r_{ss}/λ. However, as shown in Fig. 16(b), GCV provides very small regularisation parameters at certain non-dimensional source spacings. Interestingly, these non-dimensional source spacings r_{ss}/λ are the same values as the experimental model with the hemispherical sensor array becoming optimally conditioned (i.e., $\kappa(\mathbf{G}_{\mathrm{H}}) \approx 1$ when $r_{ss}/\lambda = 0.5$). In such cases, the solution will be dominated completely by errors since the problem becomes extremely well conditioned. Similar trends have been found in the simulation results shown in Figs. 11(b) and (c) under similar conditions although the geometry for the experimental model does not agree exactly with the simulated model.

In more detail, when, for example $r_{ss}/\lambda = 0.693$ in Fig. 16(b), GCV computes too small a regularisation parameter compared with β_{MSE} as shown in Fig. 17(a) and thus results in producing an "under-regularised" source strength provided by β_{GCV}. For example, as illustrated in Fig. 17(b), the strength of the unknown source reconstructed in magnitude is larger than that produced with β_{LCV} in Fig. 17(c), even though the location of unknown real source can be

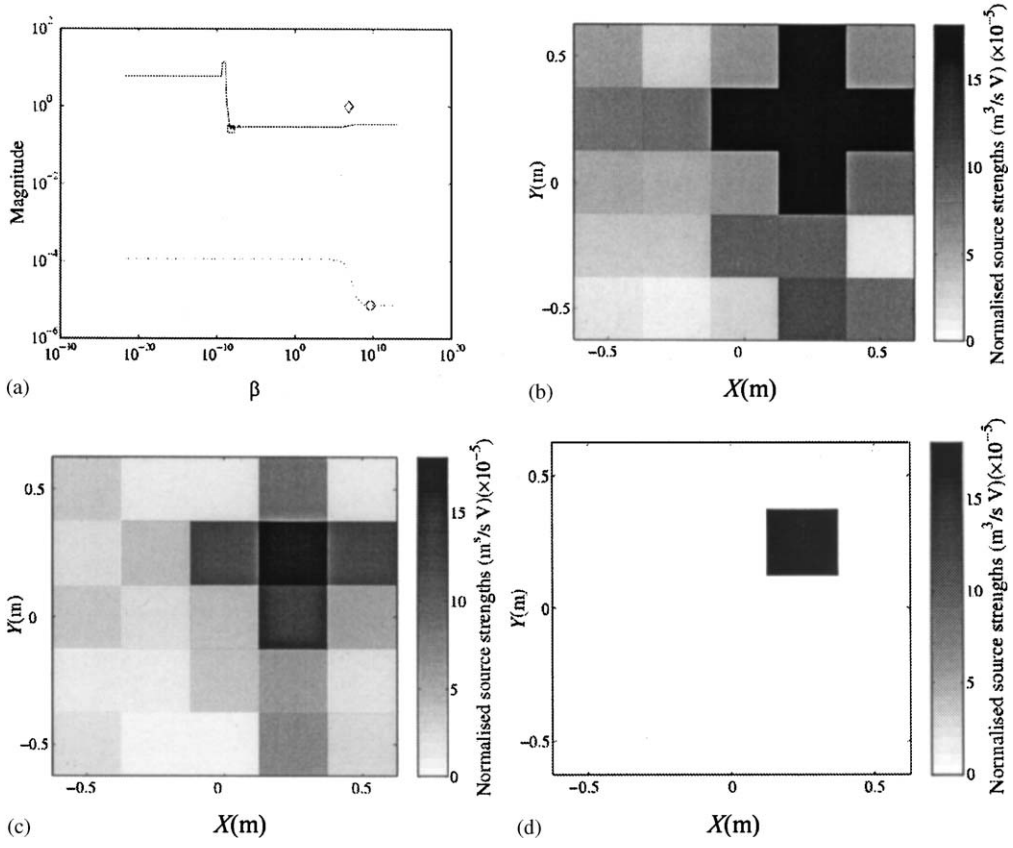

Fig. 17. Reconstruction results produced by Tikhonov regularisation, when $r_{ss}/\lambda = 0.693$ (925.8 Hz) and the radiated field, which is measured with the hemispherical sensor array, is generated by only one real acoustic source: (a) comparison between β_{MSE} (○), β_{GCV} (□) and β_{LCV} (◇); (b) source distribution at $\beta = \beta_{GCV}$; (c) source distribution at $\beta = \beta_{LCV}$; (d) true source distribution.

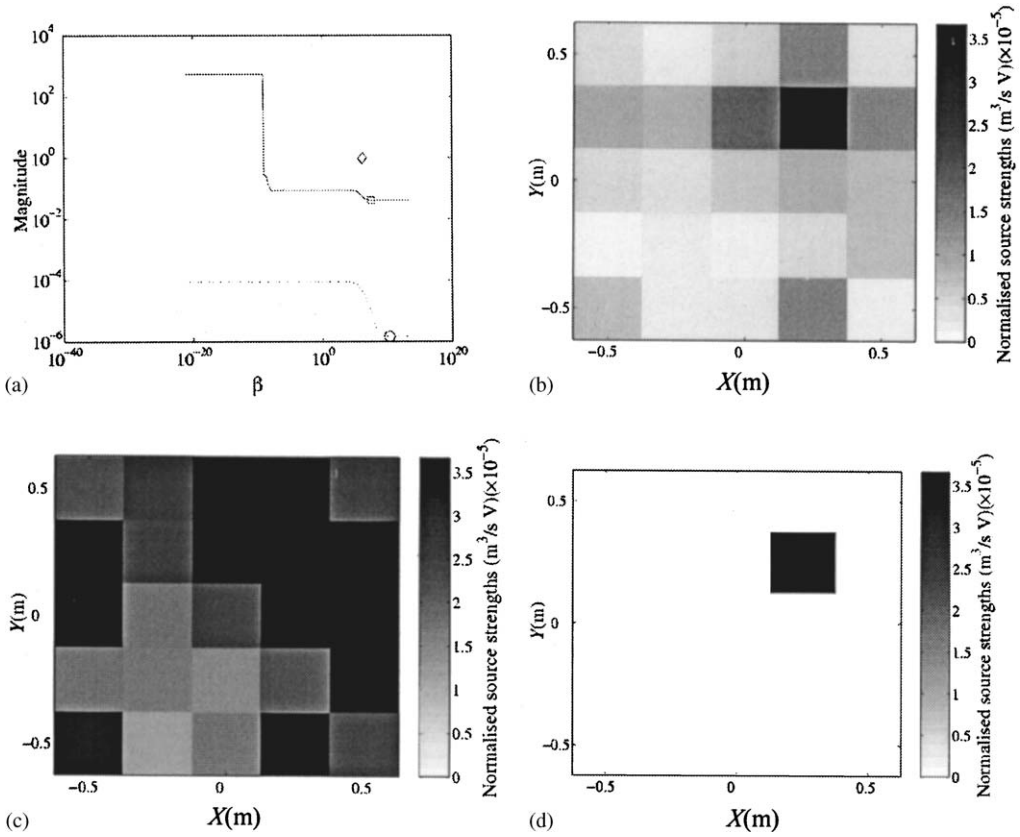

Fig. 18. Reconstruction results produced by Tikhonov regularisation, when $r_{ss}/\lambda = 0.912$ (1218.8 Hz) and the radiated field, which is measured with the hemispherical sensor array, is generated by only one real acoustic source: (a) comparison between β_{MSE} (○), β_{GCV} (□) and β_{LCV} (◇); (b) source distribution at $\beta = \beta_{GCV}$; (c) source distribution at $\beta = \beta_{LCV}$; (d) true source distribution.

revealed by the use of β_{GCV} compared with the true source distribution in Fig. 17(d). However, in contrast to the results in Fig. 17, when $r_{ss}/\lambda = 0.912$ in Fig. 18, GCV can be a better method for the determination of the regularisation parameter. This results in demonstrating very accurate reconstructions as illustrated in Fig. 18(b) compared with that for true source distribution as shown in Fig. 18(d).

As shown in Fig. 19, when the radiated sound field is generated by two real acoustic sources, similar trends to the case with one real source can be found. In other words, GCV predicts too small a regularisation parameter when the problem becomes well conditioned. It is clearly evident from Fig. 20 that in this case the small magnitude of β_{GCV} produces an under-regularised reconstruction of source distribution when the problem has very small condition number $\kappa(\mathbf{G}_H)$ afforded with the hemispherical sensor array. However, as shown in Fig. 21, in other cases GCV produces more successful reconstruction results than the L-curve method as a result of the proper determination of β_{GCV}.

In the cases for the planar sensor array with one real source (Fig. 22(a)) and two real sources (Fig. 22(b)), similarly to the case for the hemispherical sensor array, GCV seems to be more

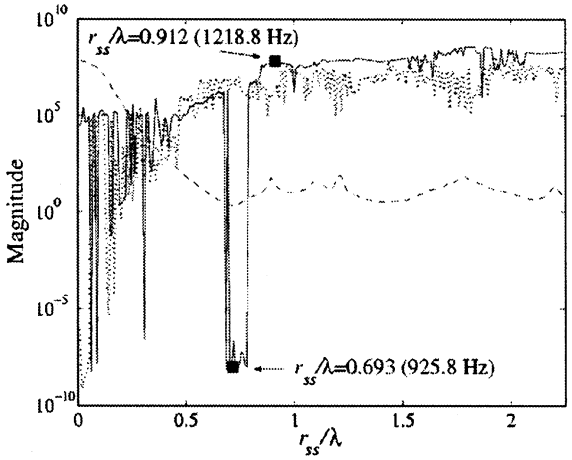

Fig. 19. Magnitude variations of the condition number and the regularisation parameters, when the radiated field, which is measured with the hemispherical sensor array, is generated by one real acoustic source (solid line, $\beta = \beta_{GCV}$; dotted line, $\beta = \beta_{LCV}$; dashed line, $\kappa(\mathbf{G}_{\mathrm{H}})$).

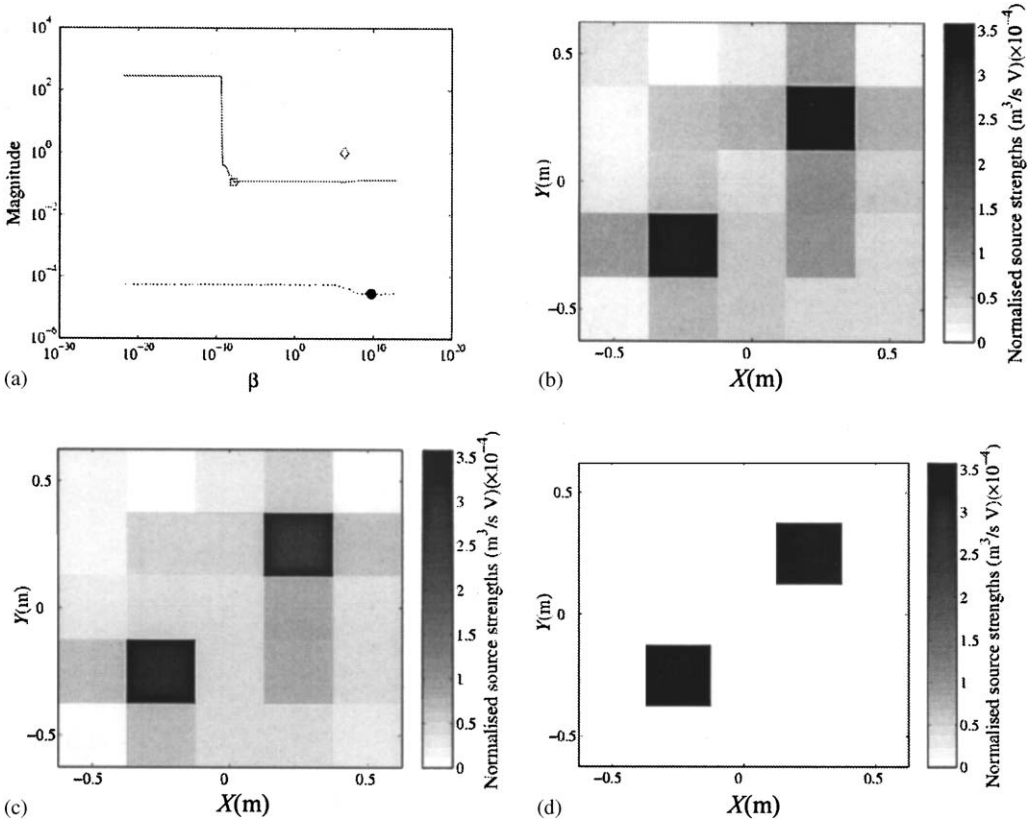

Fig. 20. Reconstruction results produced by Tikhonov regularisation, when $r_{ss}/\lambda = 0.693$ (925.8 Hz) and the radiated field, which is measured with the hemispherical sensor array, is generated by two real acoustic source: (a) comparison between β_{MSE} (○), β_{GCV} (□) and β_{LCV} (◇); (b) source distribution at $\beta = \beta_{GCV}$; (c) source distribution at $\beta = \beta_{LCV}$; (d) true source distribution.

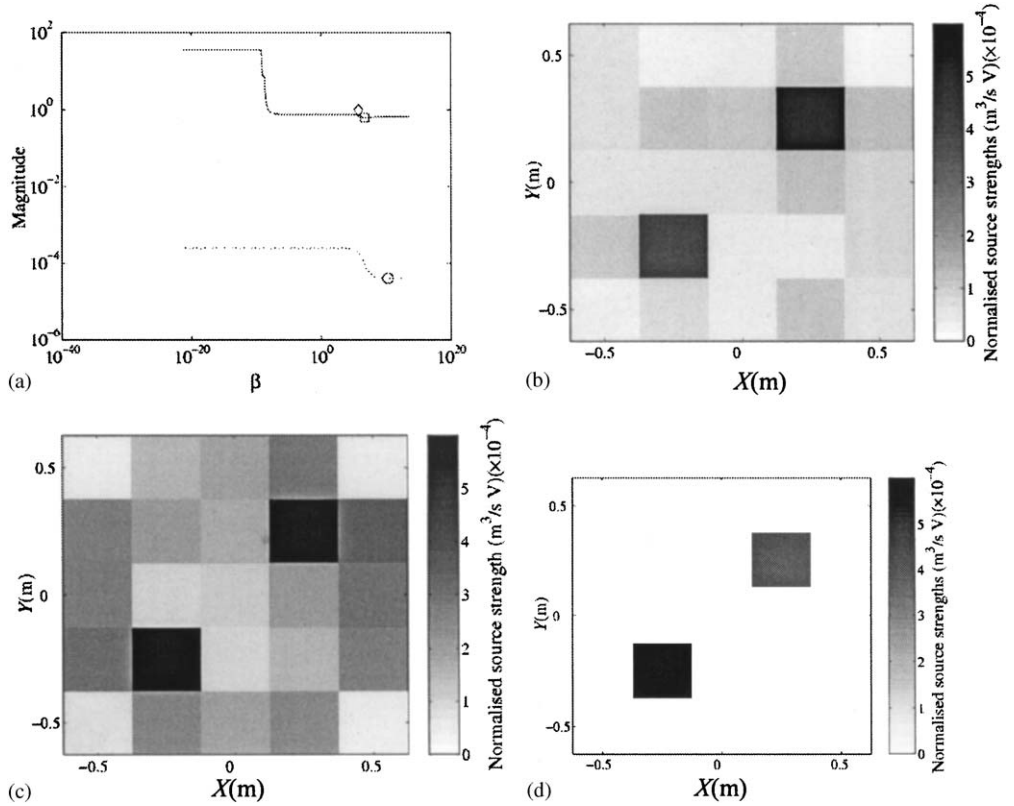

Fig. 21. Reconstruction results produced by Tikhonov regularisation, when $r_{ss}/\lambda = 0.912$ (1218.8 Hz) and the radiated field, which is measured with the hemispherical sensor array, is generated by two real acoustic sources: (a) comparison between β_{MSE} ($\bigcirc$), β_{GCV} ($\square$) and β_{LCV} ($\diamond$); (b) source distribution at $\beta = \beta_{GCV}$; (c) source distribution at $\beta = \beta_{LCV}$; (d) true source distribution.

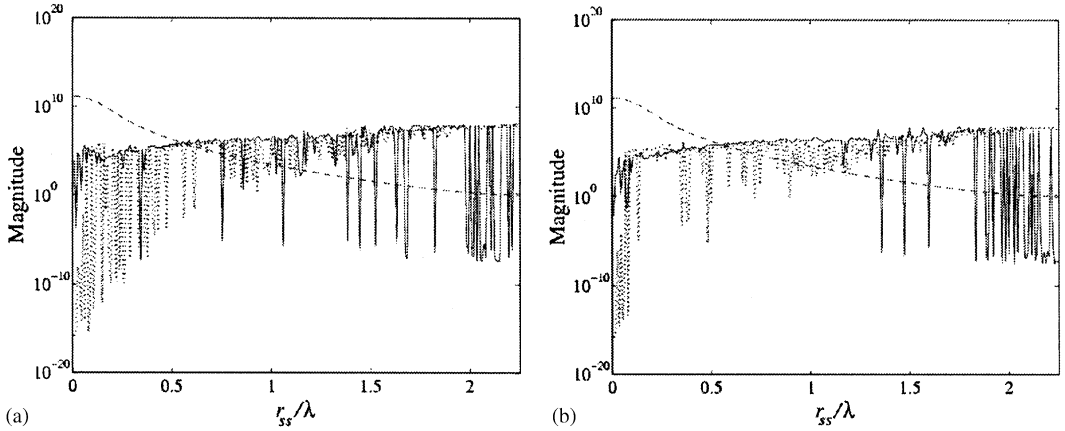

Fig. 22. Magnitude variations of the condition number and the regularisation parameters determined by GCV and the L-curve method for the planar sensor array (a) when the radiated field is generated by one real source and (b) when the radiated field is generated by two real sources. Key: solid line, $\beta = \beta_{GCV}$; dotted line, $\beta = \beta_{LCV}$ and dashed line, $\kappa(\mathbf{G}_P)$.

robust than the L-curve in the region with relatively high condition number $\kappa(\mathbf{G}_P)$ of the planar sensor array. But GCV fails to provide proper regularisation parameters in the region mainly dominated by errors since the chosen regularisation parameters are too small. Conversely, the L-curve method works well particularly in the regions completely dominated by measurement errors.

Therefore, based on the results presented, there seems to be no best method for determining proper regularisation parameters in all situations. However, in the cases investigated, GCV can be more reasonable when the problem becomes relatively ill-conditioned with contaminating noise, whilst the L-curve method may provide an effective method when the reconstructed results are mainly dominated by noise contamination.

5. Conclusions

An approach based on SVD has been applied for dealing with acoustical inverse problems when cast in the form of a Tikhonov regularisation problem. The abilities of two different methods, GCV and the L-curve method, for the determination of the proper degree of regularisation have been simulated for a wide range of acoustical conditions in conjunction with sensor and source geometries. Based on the results of the numerical simulations, it appears that GCV may be a better choice for estimating optimal regularisation parameters since GCV provides a more reasonable amount of regularisation for ill-conditioned problems when noise levels are relatively low. However, the L-curve method seems to be a more effective method when the problem is relatively well-conditioned and the reconstruction result is mainly dominated by errors such as contaminating noise. The results of the numerical simulations have also been experimentally demonstrated under laboratory conditions. Therefore, even though the cases investigated in this paper demonstrate that there is no absolutely better method, the results presented here may become useful guidelines for the right choice of regularisation parameter-determination method in real-world applications. It has also been shown however, that the optimally arranged sensor array suggested gives far superior results to those produced by a planar sensor array spanning an equivalent dimension.

References

[1] W.A. Veronesi, J.D. Maynard, Digital holographic reconstruction of sources with arbitrarily shaped surfaces, *Journal of the Acoustical Society of America* 85 (2) (1989) 588–598.

[2] G.T. Kim, B.H. Lee, 3-D sound reconstruction and field projection using the Helmholtz integral equation, *Journal of Sound and Vibration* 136 (1990) 245–261.

[3] D.M. Photiadis, The relationship of singular value decomposition to wave-vector filtering in sound radiation problems, *Journal of the Acoustical Society of America* 88 (1990) 1152–1159.

[4] S.H. Yoon, Reconstruction of Acoustic Source Strength Distributions and their Interactions by Inverse Techniques, PhD Thesis, University of Southampton, 1998.

[5] P.A. Nelson, S.H. Yoon, Estimation of acoustic source strength by inverse methods: Part I, conditioning of the inverse problem, *Journal of Sound and Vibration* 233 (4) (2000) 639–664.

[6] P.A. Nelson, A review of some inverse problems in acoustics, *International Journal of Acoustics and Vibration* 6 (3) (2001) 118–134.

[7] Y. Kim, P.A. Nelson, Spatial resolution limits for the reconstruction of acoustic source strength by inverse methods, *Journal of Sound and Vibration* 265 (3) (2003) 583–608.
[8] Y. Kim, Spatial Resolution Limits for the Reconstruction of Acoustic Source Distribution by Inverse Techniques, PhD Thesis, University of Southampton, 2002.
[9] P.A. Nelson, Y. Kim, Optimal conditioning of inverse problems in acoustic radiation, *Proceedings of 17th International Congress on Acoustics* (Book of Abstracts), 2001, 94pp.
[10] S.P. Grace, H.M. Atassi, W.K. Blake, Inverse aeroacoustic problem for a streamlined body, Part 1: Basic formulation, *American Institute of Aeronautics and Astronautics Journal* 34 (1996) 2233–2240.
[11] B.-K. Kim, J.-G. Ih, On the reconstruction of the vibro-acoustic field over the surface enclosing an interior space using the boundary element method, *Journal of the Acoustical Society of America* 100 (1996) 3003–3016.
[12] S.H. Yoon, P.A. Nelson, Estimation of acoustic source strength by inverse methods: Part II, experimental investigation of methods for choosing regularisation parameters, *Journal of Sound and Vibration* 233 (4) (2000) 665–701.
[13] Y. Kim, P.A. Nelson, Regularisation methods for acoustic source reconstruction, *Proceedings of InterNoise 2000* 1 (2000) 128–132.
[14] E.G. Williams, Regularisation methods for near-field acoustical holography, *Journal of the Acoustical Society of America* 110 (4) (2001) 1976–1988.
[15] G. Wahba, Practical approximate solutions to linear operator equations when the data are noisy, *SIAM Journal of Numerical Analysis* 14 (1977) 651–667.
[16] G.H. Goulb, M. Health, G. Wahba, Generalised cross-validation as a method for choosing a good ridge parameter, *Technometrices* 21 (1979) 215–223.
[17] G. Wahba, *Spline Models for Observation Data: CBMS-NSF Regional Conference Series in Applied Mathematics*, SIAM, Philadelphia, PA, 1990.
[18] P.C. Hansen, *Rank-Deficient and Discrete Ill-posed Problems: Numerical Aspects of Linear Inversion*, SIAM, Philadelphia, PA, 1998.
[19] P.C. Hansen, Analysis of discrete ill-posed problems by means of the *L*-curve, *SIAM Review* 34 (1992) 561–580.
[20] P.C. Hansen, D.P. O'Leary, The use of the *L*-curve in the regularisation of discrete ill-pose problem, *SIAM Journal of Science and Computing* 14 (1993) 1487–1503.
[21] A.N. Tikhonov, Solution of incorrectly formulated problems and the regularisation method, *Soviet Mathematics DOKL* 4 (1963) 1035–1038.
[22] A.N. Tikhonov, V.Y. Arsenin, *Solutions of Ill-Posed Problems*, Winston, Washington, DC, 1977.
[23] S. Barnett, *Matrices: Methods and Applications*, Oxford University Press, Oxford, 1990.
[24] P.A. Nelson, S.J. Elliott, *Active Control of Sound*, Academic Press, London, 1992.
[25] S.J. Elliott, C.C. Boucher, P.A. Nelson, The behaviour of a multiple channel active control-system, *IEEE Transactions on Signal Processing* 40 (1992) 1041–1052.
[26] P.C. Hansen, Regularisation tools: A Matlab package for analysis and solution of discrete ill-posed problems, *Numerical Algorithms* 6 (1994) 1–35.
[27] A. Schuhmacher, Practical application of inverse boundary element method to sound field studies of tyres, *Proceedings of InterNoise* 99 (1999).
[28] A. Schuhmacher, P.C. Hansen, Sound source reconstruction using inverse BEM, *Proceedings of InterNoise* 2001 (2001).
[29] C.R. Vogel, Non-convergence of the *L*-curve regularisation parameter selection method, *Inverse Problems* 12 (1996) 535–547.
[30] M. Hanke, Limitations of the *L*-curve method in ill-posed problems, *BIT* 36 (2) (1996) 287–301.
[31] A.M. Thompson, J.W. Kay, M. Titterington, A cautionary note about crossvalidatory choice, *Journal of Statistics and Computational Simulation* 33 (1989) 199–216.